Journal of Alloys and Compounds 805 (2019) 942–946

Contents lists available at ScienceDirect

Journal of Alloys and Compounds

journal homepage: http://www.elsevier.com/locate/jalcom

Al–Cu–Fe quasicrystals as the anode for lithium ion batteries

Xiao Lan [a, b, c, d], Haijuan Wang [a, b, c, d], Zhanhao Sun [a, b, c, d], Xunyong Jiang [a, b, c, d, *]

[a] Key Laboratory of Display Materials and Photoelectric Devices, Ministry of Education, China
[b] Tianjin Key Laboratory for Photoelectric Materials and Devices, China
[c] National Demonstration Center for Experimental Function Materials Education, China
[d] School of Materials Science and Engineering, Tianjin University of Technology, Tianjin, China

ARTICLE INFO

Article history:
Received 26 October 2018
Received in revised form
26 June 2019
Accepted 15 July 2019
Available online 15 July 2019

Keywords:
Li-ion battery
Al–Cu–Fe
Quasicrystal
Anode

ABSTRACT

In this paper, Al–Cu–Fe quasicrystal alloy was used as the anode material for lithium-ion batteries. The first specific discharge capacity of quasicrystal was 204 mA h/g. Cyclic voltammetry showed that the oxidation peak of the Al–Cu–Fe quasicrystal was at about 1.4 V. The reduction peak was at 0.3 V. The Al–Cu–Fe quasicrystals had a higher Li-ion diffusion impedance and Warburg impedance in the first cycle. X-ray diffraction analysis demonstrated that Li atoms enter into the quasicrystal structure and can-not fully leave the quasicrystal during the first charge-discharge cycle, which induces an irreversible capacity.

1. Introduction

Lithium-ion batteries (LIBs) are considered to be state-of-the art energy storage systems due to their high gravimetric and volumetric energy densities. However, the energy density of the current LIBs can not satisfy the ever-growing demands for electric vehicles (EVs), portable electronics and large-scale renewable energy storage [1]. Compared with commercial graphite anodes (372 mA h/g) with an intercalation reaction mechanism, higher lithium storage capacity could be achieved with metallic or semi metallic elements (Al, Si, Ge, Sn, Sb, etc.) or with MaXb-type compounds (where M is a transition metal and X being F, O, P, N, S …)by an alloying reaction or conversion reaction with lithium, respectively [2]. Silicon-based anodes have the advantages of high capacity and low charge potential. However, the large volume expansion (300%) and the continuous formation of an SEI film during the delithiation process seriously hinder the practical application of silicon-based anodes. The application of other materials is limited by low cycle property, and low coulomb efficiency. The search for a new environmentally clean metallic anode is one of the important technical routes to developing high energy LIBs [3].

Quasicrystals (QCs) have a structure that is ordered but not periodic and present 5-fold, or even 8-fold or 10-fold symmetries [4]. The special atomic arrangement of QCs determine its special property. QCs have been used as hydrogen storage materials, such as gas storage and electrochemical hydrogen storage [5,6]. Al–Cu–Fe can form QC by direct melt casting process [7]. Al–Cu–Fe QCs, such as $Al_{63}Cu_{25}Fe_{12}$, contain a large portion of aluminum which has a high lithium storage capacity. Al–Cu–Fe QCs may store lithium reversibly. To the best of our knowledge, there has been no study on the lithium storage of Al–Cu–Fe QCs. In this paper, $Al_{63}Cu_{25}Fe_{12}$ was prepared by the general melt casting method and high-energy ball milling. The lithium storage property of Al–Cu–Fe QCs was studied. The results show that Al–Cu–Fe QCs have a definite lithium storage capacity.

2. Materials and methods

$Al_{63}Cu_{25}Fe_{12}$ ingot were prepared by art melting with Fe (chip 99.9%), Cu (shot 99.9%) and Al (shot 99.9%). The ingot was annealed at 800 °C for 10 h under an argon atmosphere. Then it is put into ball mill to crush into powder. The final particle size were less than 0.0374 mm. The electrodes for electrochemical test were prepared as follow: the alloy powder and PVDF were mixed with the mass ratios of 8:1. The mixture with addition of a suitable amount of N-methyl-2-pyrrolidone (NMP) were stirred with a magnetic whisk for 1 h, and pasted onto the copper foils. The materials were

* Corresponding author. Key Laboratory of Display Materials and Photoelectric Devices, Ministry of Education, China.
E-mail address: jiangxunyong@tjut.edu.cn (X. Jiang).

https://doi.org/10.1016/j.jallcom.2019.07.148
0925-8388/

punched into circular electrode slices (15 mm in diameter) after they were dry for 4 h at 25 °C. Then the electrode slices were placed on a wild mouthed Petri dish to be heated for 10 h at 120 °C in the vacuum drying oven. The average weight of the electrodes was approximately 18 mg. The mental Lithium was used as anode in the cells. And a porous polymeric membrane (Celgard 2400) was used as diaphragm. 1 M LiBF4 dissolved in EC, DEC and EMC mixture of equal volumes was used as electrolyte. The cells were assembled in an argon-filled glove box with the concentrations of moisture and oxygen below 0.1 ppm.

The samples were characterized using Rigaku D/Max-2500 V X-ray diffraction (XRD) in the range of 10°–90°. Charge-discharge cycles test of the electrodes were carried out on the NEWARE tester at 25 °C. IM6 electrochemical workstation was utilized to measure electrochemical impedance spectra (EIS) in the frequency range of 110 kHz to 0.01 Hz with AC amplitude 5 mV. Cyclic voltammetry measurements were tested at a scan rate of 0.1 mV/s in the voltage range of 0–3 V (versus Li/Li^+) and current range of −40 to 40 mA. Analyses of surface composition of the electrodes before and after cycling were conducted using XPS (Kratos-AXIS UL TRADLD, Al KaX-ray source). The morphology and elemental changes of the electrode sheets before and after the cycle were analyzed using a field emission scanning electron microscope (FESEM, JSM-6700 F).

3. Results and discussion

Fig. 1 shows the XRD patterns of Al–Cu–Fe alloy powders (a: after heating and ball milling, b: as-cast). For the as-cast alloy, there exist two diffraction peaks of icosahedral phase between 42° and 46°, which are diffraction peaks of Al–Cu–Fe QCs. The XRD peaks of QC phases become broader, and the peaks of β-Al(Cu,Fe) phase disappear, transforming into the QC phase [8,9]. The crystalline β-Al(Cu,Fe) phase is also present in the as cast alloy. After heating and high-energy ball milling, the XRD peaks of the QC phases still remain. But the peaks of the β-Al(Cu,Fe) phase disappear. These XRD results show that pure Al–Cu–Fe QCs can be obtained by heat treatment and subsequent high-energy ball milling. The following electrochemical test was performed with pure Al–Cu–Fe QCs prepared by the process that provided the Al–Cu–Fe powders whose XRD pattern is depicted in Fig. 1a.

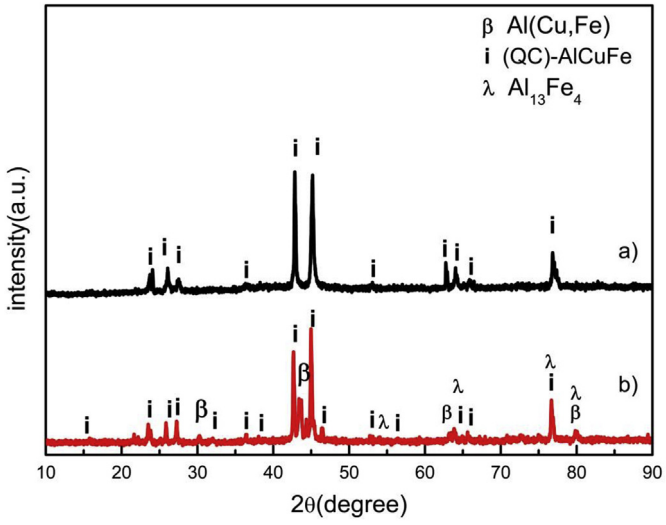

Fig. 1. XRD patterns of Al–Cu–Fe alloy powders (a: after heat treatment and ball mill, b: as cast).

To eliminate the influence on specific capacity, acetylene black was not added to the anodes as the conducting material. Fig. 2a display the charge-discharge voltage profiles of the Al–Cu–Fe QCs from the 1st to 50th cycles at a current density of 100 mA/g. In the first discharge process, there was a relatively slow discharge platform between 1.0 V and 0.5 V, corresponding to the formation of an SEI film. The tilt table at 0.25 V corresponded to the process of lithium ions embedding into the QCs material. After the 50th cycle, the platform almost disappeared. The first specific discharge and charge capacities were 204 mA h/g and 60 mA h/g, respectively. For the subsequent cycles, the specific discharge and charge capacities were almost the same (Fig. 2b). This means that an irreversible process exists during the first discharge process when Li ions react with the Al–Cu–Fe QCs.

The CV curves reveal the lithiation/delithiation process of the Al–Cu–Fe QC architecture. The reduction and oxidation peaks are clearly shown in the CV curve (Fig. 2c). In the first scan, the broad reduction peak between 0.6 V and 1.3 V is related to the formation of the SEI layer. The peaks at 0.2 V and 1.4 V are related to the intercalation/deintercalation of Li in the active materials to form $AlLi_x$, corresponding to a reversible process [10,11]. After the third scan, the broad reduction peak between 0.6 V and 1.3 V nearly disappears, indicating the formation of a stable SEI film on the anode surface. This is consistent with the charge-discharge results, in which the QCs have an oblique platform in the first cycle.

The EIS results are shown in Fig. 2d. The semicircle in the high-frequency region is ascribed to the formation of the SEI film and the process of lithium ions passing through the SEI film. The slanted line is consistent with the process of lithium ion diffusion in the anode. Initial result (designated as 0) show a higher charge transfer resistance and higher Warburg impedance than after the first and tenth cycles. With charge-discharge cycling, the semicircle and slope of the slanted line become smaller, which means that Li-ion transmission channels are opened. The electrode material structure is more suitable for intercalation/deintercalation of Li-ions. There is no significant difference between the first and tenth cycles in the semicircle, indicating that impedance of Li-ion diffusion in the materials is not significantly changed. The behaviors of Li in the QCs material anode is a combination of control of charge transfer and diffusion steps. The EIS results show that addition of acetylene black or modification of the material may improve the electrochemical performance of the anode.

The morphology and element distribution of different states of the electrode were characterized by SEM. As shown in Fig. 4, the quasi-crystalline material on the initial state electrode sheet can be clearly observed and the particle is irregular (Fig. 3a). When lithium ion is fully embedded in the negative electrode, the surface of the electrode sheet changes to form a thin layer similar to a sponge (Fig. 3c). At this time, Al in the anode material reacts with lithium ions, and the content is reduced. When discharging is over, the sponge-like thin layer on the surface of the electrode sheet was mostly removed, and the quasi-crystalline material was re-exposed and the proportion of Al element was increased again (Fig. 3b). Surface morphology of the electrode is not completely recovered with the proceeding of discharge, indicating that the reversibility at the initial stage of the cycle is poor.

XPS spectra of three samples under different state are exhibited in Fig. 4. In the wide scan XPS spectrum of the AlCuFe quasicrystal, as shown in Fig. 4a, Cu2p peak (932.4 eV), Fe2p peak (706.75 eV) and Al2p peak (72.65 eV) were observed, two peaks at 531.6 and 284.6 eV attributed to O 1s and C 1s are also showed. Compared with the original material, both curves after charging and discharging showed a new peak of Li 1s around 55.5 eV, as shown in Fig. 4a. This indicates that lithium ion reacted with the quasi-crystalline material of the negative electrode during the charging

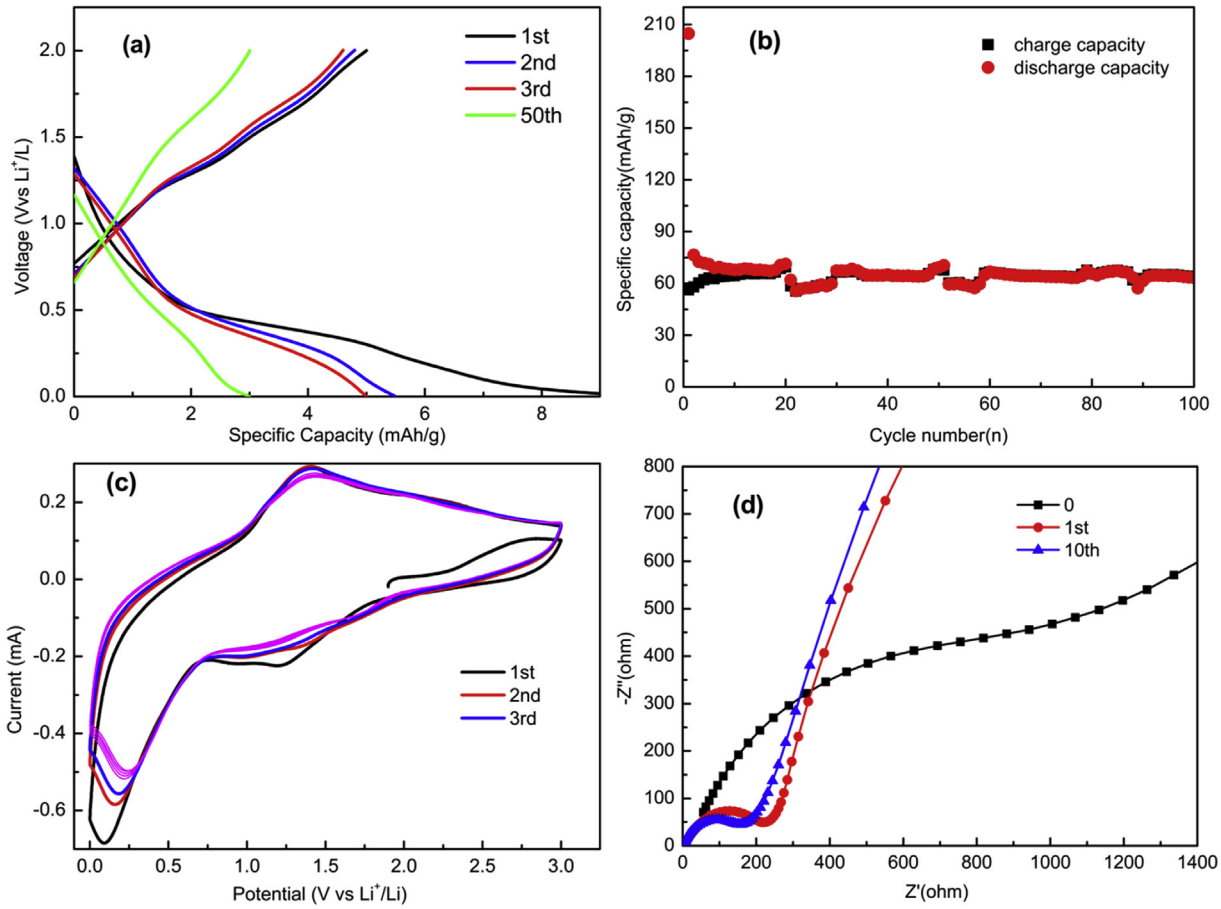

Fig. 2. Electrochemical test of Al–Cu–Fe QCs(a) charge-discharge curves. (b) cycling performance at 100 mA/g (c) CV curves. (d) Nyquist plots of QCs at an open-circuit potential with different cycle.

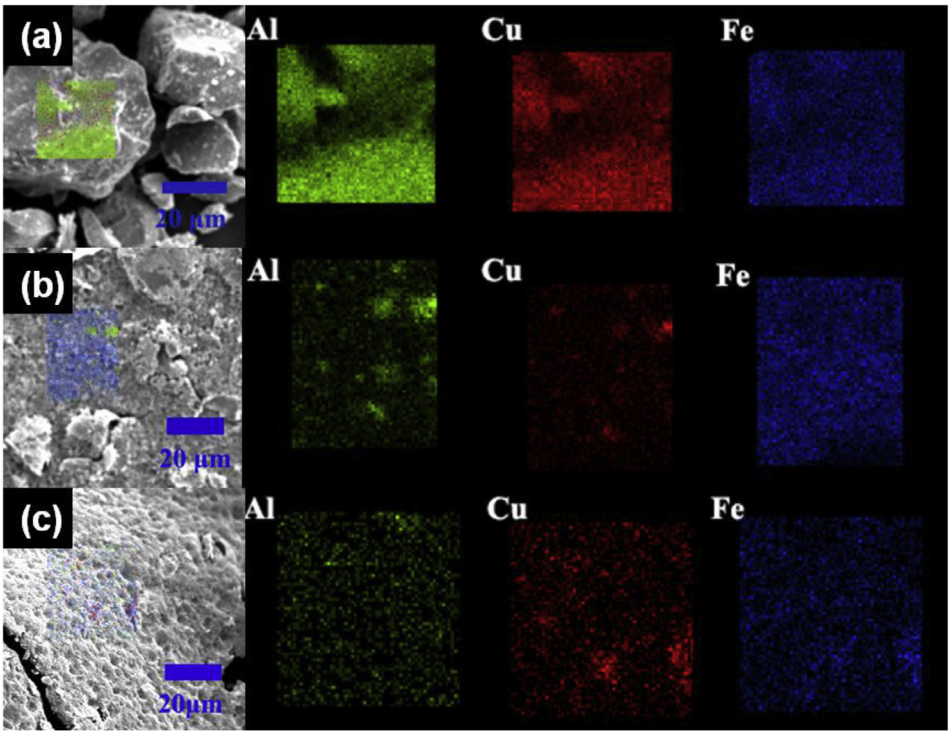

Fig. 3. SEM images and SEM-EDS mapping of Al, Cu, Fe elemental distributions on electrodes at (a) pristine, (b) fully discharged, and (c) fully recharged states.

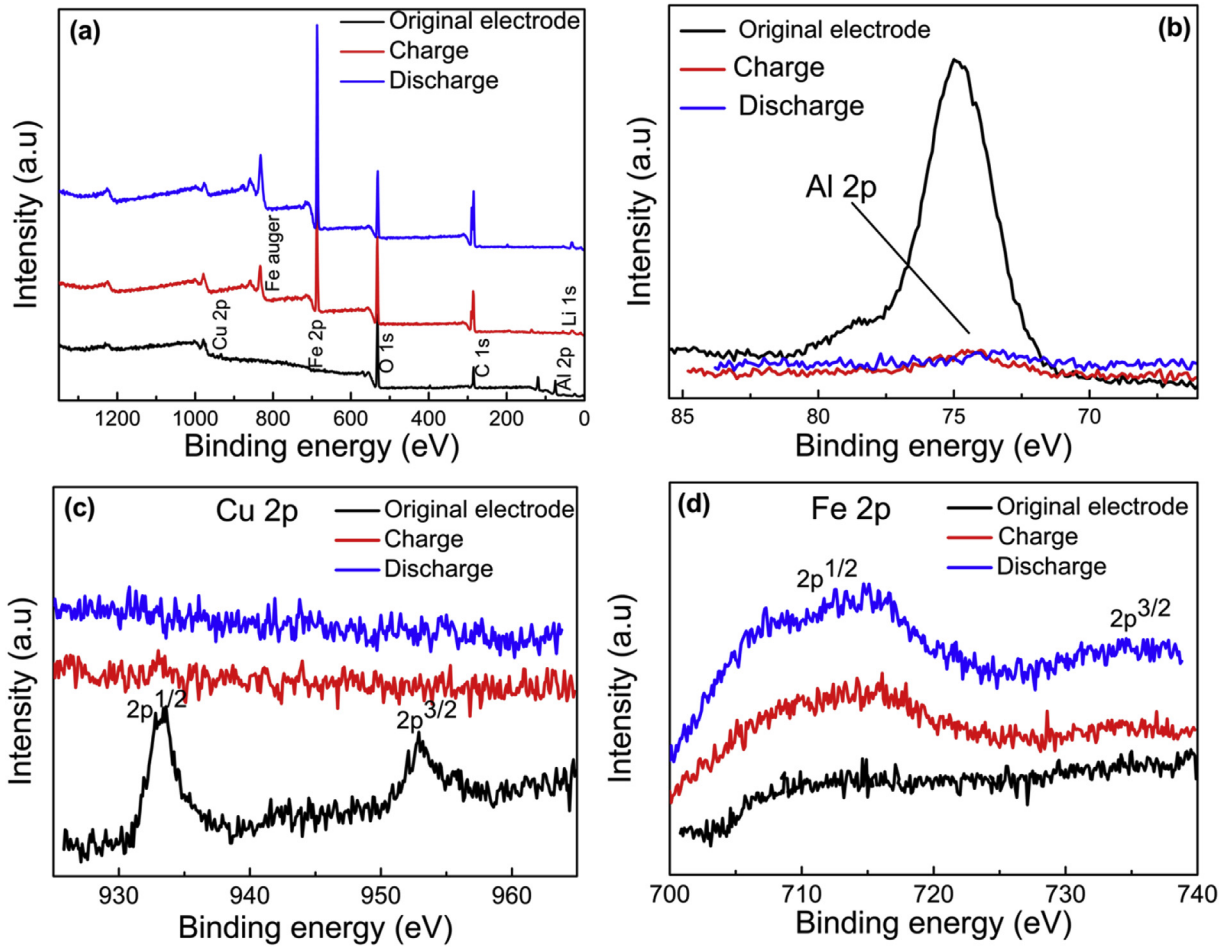

Fig. 4. (a) XPS survey spectra, (b) Al 2p spectra, (c) Cu 2p, (d) Fe 2p.

and discharging process. The peak of Li 1s after charging was higher than the peak after discharging. This means that some lithium ions are still unable to escape the alloy layer due to the occurrence of an irreversible reaction after the delithiation reaction. Fig. 4b, c, d show the XPS of Al, Cu and Fe one by one before and after the cycle. The form of Al change obviously after charging and discharging, and Fe still exists in its original form presence. The Cu element does not have lithium storage capacity. The capacity of AlCuFe quasicryatal comes from Al.

In order to observe the structure change of QCs during the charge-discharge cycle, the cell under different charge states was disassembled in a glove box. A prepared slurry was evenly coated on a nickel foam for the test battery. The electrode sheets were removed and surrounded with polyethylene film to take the XRD measurements. XRD patterns of the Al–Cu–Fe alloys in the first cycle are shown in Fig. 5 The upper right corner of Fig. 5 is the charge-discharge curve of AlCuFe QCs. Five samples subjected to XRD measurement in different charge and discharge states are shown in Fig. 5, as indicated. In order to facilitate the observation of the change in the alloy phase, we have enlarged the diffraction peaks of 44°–45° in the upper left corner of Fig. 5. The highly interfering nickel peaks have been eliminated. Curve e in Fig. 5 is the diffraction peak of the pure protective film, and curve d is the diffraction peak of the polyethylene film surrounding the QCs alloy. It is obvious that the polyethylene film does not affect the diffraction peak of the alloy electrode.

The entire charge-discharge cycle is 2 V-0 V–2 V. The half cycle

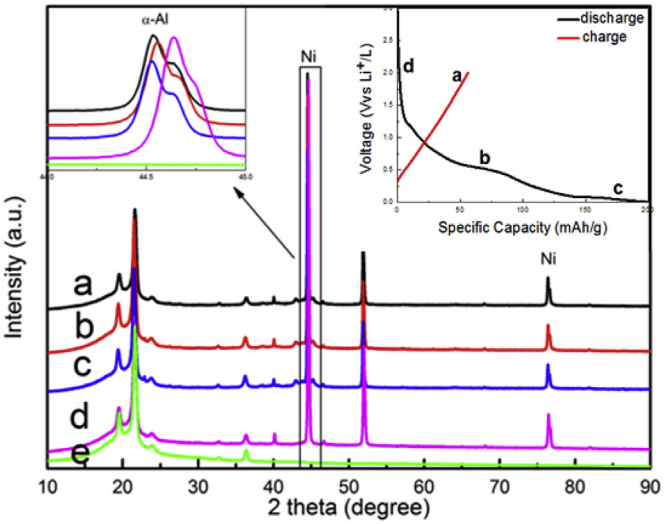

Fig. 5. XRD patterns of AlCuFe QCs in different charge-discharge state and charge-discharge curve in first cycle (upper right corner) (a: charge over, b: discharge to 0.5 V, c: discharge over, d: Polyethylene film with alloys, e: Polyethylene film).

of the lithium insertion process is from 2 V to 0 V, which is the discharge process. The intermediate point of 0.5 V is the middle state of the lithium insertion process. Combining the voltage and

XRD changes during charge and discharge, it can be seen that (curve b, c in Fig. 5) the peak of the QC phase deviates slightly from the initial position during discharge process. The peaks were shifted significantly to the left and widened compared with the alloy in its initial state (curve d in Fig. 5). When the discharge process finishes, the voltage of the anode is 0 V. The overall peak shifts toward a small angular direction, which means that the interplanar spacing increases (curve c in Fig. 5). The broadening of the diffraction peaks means a decrease in crystalline size and concentration of material stress. However, neither the intermetallic compound nor the unalloyed material appears in the diffraction pattern. This indicates that only the solid solution was present in the alloy when the lithium ions were embedded in the aluminum matrix of the ternary Al–Cu–Fe alloy. This induce the small angle movement of the α-Al peak in the XRD pattern. The half cycle is the lithium deinsertion process from 0 V to 2 V which is the charge process. When charging is completed, the voltage of the electrode returns to 2 V. The position of the diffraction peak cannot be restored to the original position (curve a in Fig. 5). This means that a portion of the lithium ions embedded in the QCs cannot be removed during the deinsertion process. As a result, irreversible capacity loss occurs. The peak shift is small throughout the process. This means that only the active substances in the surface layer may participate in the reaction.

4. Conclusions

In this paper, Al–Cu–Fe QCs were synthesized by melting and subsequent heat treatment. The electrochemical performance of AlCuFe QCs as anodes of LIBs was tested.

1) $Al_{63}Cu_{25}Fe_{12}$ QCs can store lithium reversibly. There exist the irreversible process during the first discharge process. The first specific discharge capacities were 204 mA h/g, dropping to 65 mA h/g after 50 cycles.
2) The cyclic voltammogram showed the oxidation peak of Al–Cu–Fe QCs at about 1.4 V, and the reduction peak at 0.3 V. EIS measurements revealed that the material showed higher Li-ion diffusion impedance and Warburg impedance in the first cycle.
3) During discharging process, lithium ions penetrate into the QCs to form a solid solution. During the charging process, a portion of the lithium atoms can-not leave the QCs, which causes irreversible capacity.

References

[1] W.J. Zhang, J. Power Sources 196 (2011) 13–24.
[2] M.M. Thackeray, J.T. Vaughey, L.M. Fransson, J. JOM. 54 (2002) 20–23.
[3] M. Wachtler, M. Winter, J.O. Besenhard, J. Power Sources 105 (2002) 151–160.
[4] D. Rouxel, P. Pigeat, J. Progress. Surf. Sci. 81 (2006) 10–12.
[5] X.Y. Jiang, L. Zhang, R. Zhang, J. Chin. Rare Met. 36 (2012) 248.
[6] Xuanli Luo, D.M. Grant, G.S. Walker, J. Alloy. Comp. 645 (2015) S23–S26.
[7] A. Peter, Bancel. Philos. Mag. Lett. 67 (1) (1993) 43–49.
[8] B.P. Dhonge, D.E. Motaung, C.P. Liu, J. Sensors Actuators B Chem. 215 (2015) 30–38.
[9] S. Zhang, K. Zhao, T. Zhu, J. Prog. Mater. Sci. 89 (2017) 479–521.
[10] M.N. Obrovac, V.L. Chevrier, J. Chem. Rev. 114 (2014) 444–502.
[11] P. Verma, P. Maire, P. Novák, J. Electrochem. Acta 55 (2010) 6332–6341.